Supporting information

Improving combination cancer immunotherapy by manipulating dual immunomodulatory signals with enzyme-triggered, cell-penetrating peptide-mediated biomodulators

Guibin Pang[a], Piao Chen[a], Xuewei Cao[a,c], Huan Yu[e], Leshuai W. Zhang[e], Jian Zhao[a,c,], Fu-Jun Wang[b,c,d,*]*

a. State Key Laboratory of Bioreactor Engineering, East China University of Science and Technology, 130 Meilong Road, Shanghai 200237, P. R. China. Email: zhaojian@ecust.edu.cn

b. New Drug R&D Center, Zhejiang Fonow Medicine Co., Ltd., 209 West Hulian Road, Dongyang 322100, Zhejiang, P. R. China.

c. ECUST-FONOW Joint Research Center for Innovative Medicines, East China University of Science and Technology, 130 Meilong Road, Shanghai 200237, P. R. China.

d. Institute of Chinese Materia Medica, Shanghai University of Traditional Chinese Medicine, 1200 Cailun Road, Shanghai 201203, P. R. China. Email: wfj@shutcm.edu.cn

e. School for Radiological and Interdisciplinary Sciences (RAD-X), State Key Laboratory of Radiation Medicine and Protection, School of Radiation Medicine and Protection, Collaborative Innovation Center of Radiation Medicine of Jiangsu Higher Education Institutions, Soochow University, Suzhou 215123, China

Sequences of the proteins and peptides

BLF1

PNSLEAQIRQAMKTGSTLTIEFDQALNQKSPGTLNVFLHPANGGVRIDLDSGNQGEPAKILWLPWIQGELQ
TLQPGSISTVDMLFFTYYLSGCKVFAGDGGPIWHIDAPVEANQFWRRMSSDEWMEDWEVGTDRQVAYL
HRAGQSDSLWNLSAYLEGAAPSTYGRDNLGQAVVGGIVTGRQQMSLYQYATTSSGSSAWSPLTYTLQQ
RKQ

D3

VDGTGMGSDLGKKLLEAARAGQDDEVRILMANDAFGDTALHLAADWGHPEIVKILLLQPGGDVDANG
DTALHLAAKNGHPEIVKILLLQPGGDVDAHGNTALHLAAVTGHPEIVKILLLQPGGDVDAQDKFGKTAF
DISIDNGNEDLAEILQLE

Pb-binding domain

KARKVRFSEKVTVHFL

KVxF

KARKVRFSEKV

ΦΦ

TVHFL

C6H

KLKRKKKGKGLGKKRDPCLRKY

RGDK*3

RGDKRGDKRGDK

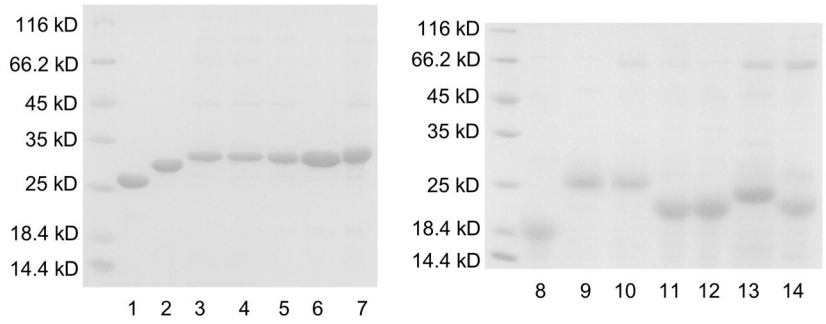

Fig. S1. SDS-PAGE analysis of the chimeric proteins stained with Coomassie brilliant blue. Lane 1, BLF1; lane 2, BC; lane 3, BPC1; lane 4, BPC2; lane 5, BPC3; lane 6, BPR; lane 7, RBPC; lane 8, DΦ; lane 9, DΦC1; lane 10, DΦC2; lane 11, DΦ3R1; lane 12, DΦ3R2; lane 13, ΦCD; lane 14, Φ3RD.

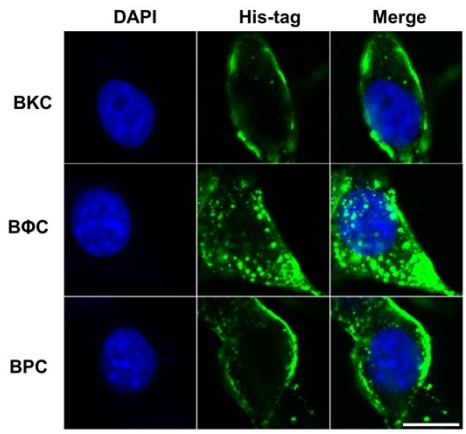

Fig. S2. Immunofluorescence image of the internalized biomodulator BKC, BΦC and BPC (1 μM). Scale bar is 10 μm.

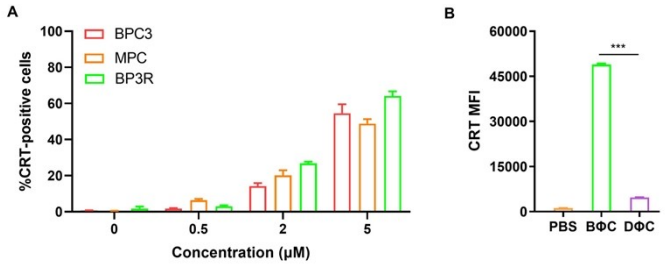

Fig. S3. Surface CRT exposure following chimera treatment. (A) CT26 cells were treated with BPC3, MPC and BPR3R (0.5, 2, 5 μM), (B) BΦC and DΦC (5 μM) for 12 h. MPC contained another ribosome-inactivating protein MAP30. Data represent mean ± SD. ***P<0.001.

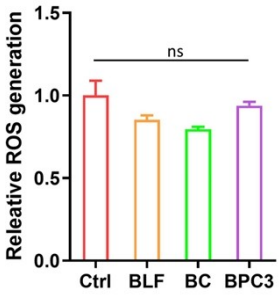

Fig. S4. The relative production of ROS after the treatment of 5 μM BGC for 24 h. Data represent mean ± SD. ns, not significant.

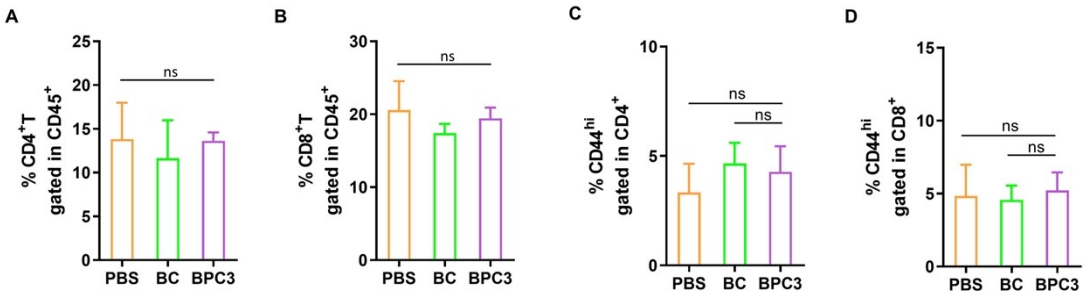

Fig. S5. Percentage of (A) $CD4^+$ T cells, (B) $CD8^+$ T cells and (C) $CD44^+$ gated in $CD4^+$ T cells in lymph node. (D) Percentage of $CD44^+$ gated in $CD8^+$ T cells in spleen. Data represent mean ± SD. ns, not significant.

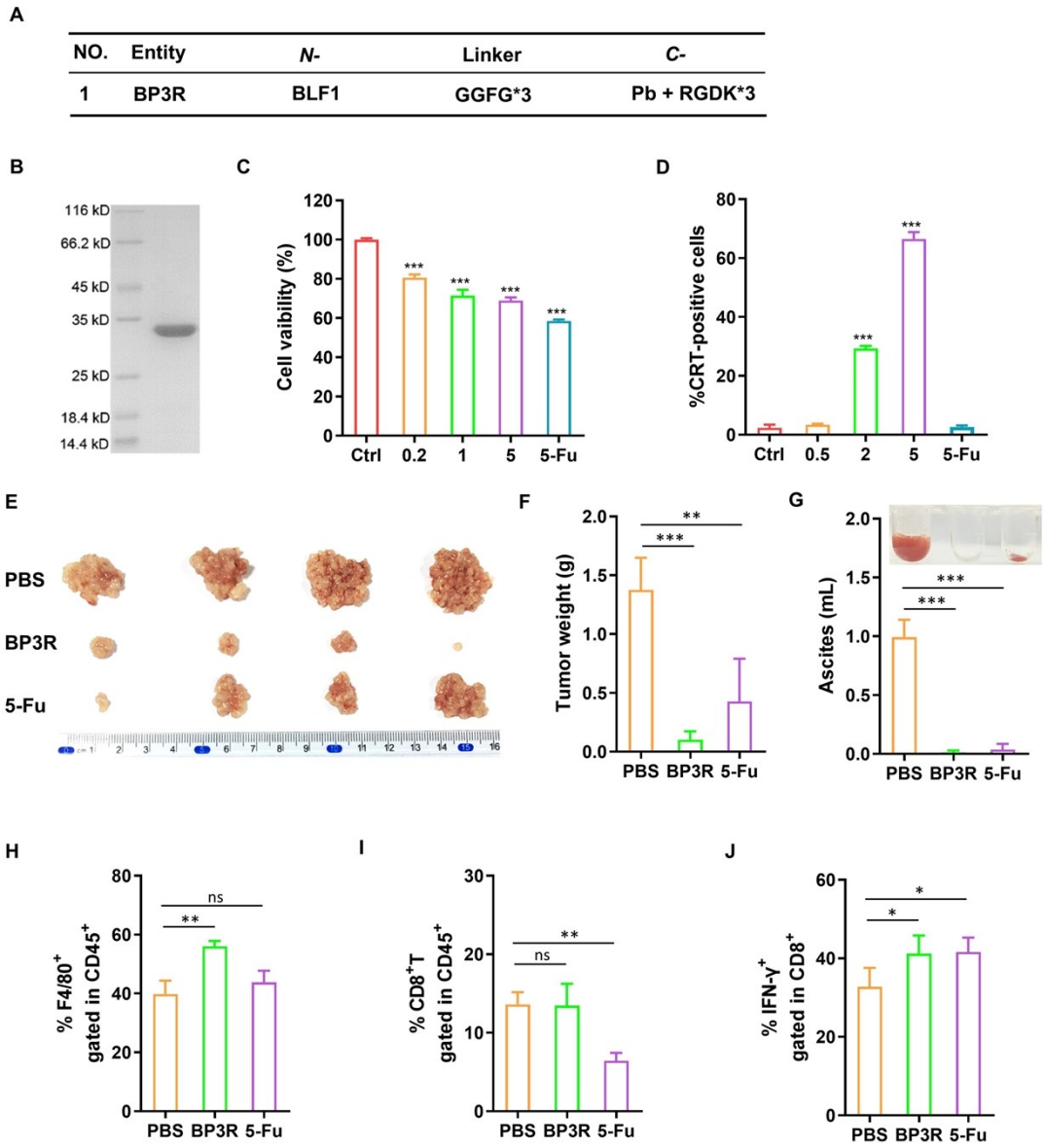

Fig. S6. Antitumor effect of the tumor-specific biomodulator BP3R. (A) Structural representation of biomodulator BP3R. (B) SDS-PAGE analysis of BP3R stained with Coomassie brilliant blue. (C) Cytotoxicity of BG3R against CT26 tumor cells. (D) CRT exposure after the treatment of BG3R at various concentrations. (E) Representative images of disseminated tumor from peritoneal cavity. (F) Quantitative analysis of tumor weight. (G) Quantitative analysis of ascites volume. (H) Flow cytometric analysis of the infiltration of macrophage and (I) $CD8^+$ T cells in tumors, and (J) the production of IFN-γ in $CD8^+$ T cells. Data represent mean ± SD. ns, not significant. *P<0.05, **P<0.01, ***P<0.001.

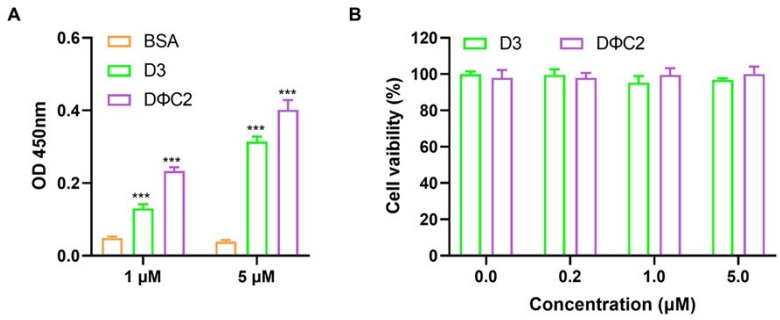

Fig. S7. Functional analysis of D3-based biomodulator. (A) Protein-level analysis of the PD-L1 binding affinity of D3-based biomodulator. (B) Cytotoxicity of the biomodulator against CT26 tumor cells.